Article:
Zare Pakzad, Sina, Nasr Esfahani, Mohammad orcid.org/0000-0002-6973-2205, Canadinc, Demircan et al. (1 more author) (2025) Machine learning-driven atomistic analysis of mechanical behavior in silicon nanowires. Computational Materials Science. 113446. ISSN 0927-0256

https://doi.org/10.1016/j.commatsci.2024.113446

Machine Learning-Driven Atomistic Analysis of Mechanical Behavior in Silicon Nanowires

Sina Zare Pakzad[a], Mohammad Nasr Esfahani[b], Demircan Canadinc[c], B. Erdem Alaca[a,d,e,*]

[a]*Department of Mechanical Engineering, Koç University, Rumelifeneri Yolu, 34450 Sariyer, Istanbul, Turkey*
[b]*School of Physics, Engineering and Technology, University of York, York, YO10 5DD, UK*
[c]*Advanced Materials Group (AMG), Department of Mechanical Engineering, Koç University, 34450, Istanbul, Turkey*
[d]*n²STAR-Koç University Nanofabrication and Nanocharacterization Center for Scientific and Technological Advanced Research, Koç University, Rumelifeneri Yolu, 34450 Sariyer, Istanbul, Turkey*
[e]*Koç University Surface Technologies Research Center (KUYTAM), Koç University, 34450 Sariyer, Istanbul, Turkey*

Abstract

This study investigates the modulus of elasticity of silicon nanowires using a combination of molecular dynamics simulations and machine learning techniques. The research presents a substantial dataset with over 3000 data points obtained from molecular dynamics simulations, which reveals detailed insights into the mechanical properties of silicon nanowires and underscores the importance of accurate model calibration. Machine learning surrogate models are employed to predict the elasticity of silicon nanowires, focusing on the influence of surface state and crystal orientation. By analyzing partial dependencies and using inverse pole figures, the study demonstrates that the modulus of elasticity exhibits significant orientation dependence. This work bridges computational and experimental approaches, offering a refined understanding of the mechanical behavior of silicon nanowires. The findings highlight the potential of integrating machine learning with atomistic simulations to improve the predictive accuracy of material properties, building the framework for advancements in nanoelectromechanical applications.

Keywords: Silicon nanowire, molecular dynamics, machine learning, tensile behavior, modulus of elasticity

1. Introduction

Nanowires (NWs) exhibit a significant potential as essential building blocks for the development of nanoelectromechanical systems (NEMS) [1], nanoelectronics [2], and photonics [3, 4] with applications as highly sensitive sensors [5] and energy-related technologies [6, 7]. Significant advancements in fabrication techniques and the wider range of technological applications have generated increased interest in thoroughly characterizing NWs [8, 9, 10]. The utilization of multi-scale modeling methods also contributes to this growing interest [11, 12].

The surface contribution becomes more significant as a result of a size reduction in nanomaterials leading to different physical properties compared to the bulk counterpart [13, 14]. The mechanical properties are found to be considerably size-dependent at nanoscale [13, 15, 16]. Hence understanding the mechanical behavior of NWs is essential to embed them into NEMS devices [16, 17]. Various experimental methods are employed to investigate the impact of size reduction on the mechanical properties of NWs. This includes studying the modulus of elasticity, fracture strength, and brittle to ductile transition temperature, where considerable changes in the mechanical properties have been identified as a result of size reduction [11, 12, 16, 18]. Thus nanomechanical modeling techniques have been developed as a means to explain such behavior in NWs [12]. These approaches can be classified as continuum mechanics, analytical models, atomistic simulations and first principle methods providing in-depth analysis on the scale effect [11, 12, 17, 19, 20]. As the size decreases, the surface contribution becomes more prominent, leading to notable size-dependent properties of the NWs [11, 12, 21, 22]. In this respect, understanding the scale effect becomes more challenging [11, 12, 22, 23].

Silicon (Si) NWs have been extensively investigated as fundamental components in semiconductor manufacturing due to their unique properties [13, 16, 24, 25, 26]. Although there have been numerous investigations into the size-dependent mechanical properties of Si NWs, conflicting findings highlight

*Corresponding author
Email address: ealaca@ku.edu.tr (B. Erdem Alaca)

the need for a more comprehensive analysis of the scale effect [11, 12, 15, 22]. A recent study highlights the necessity of adopting a multiscale theoretical framework to gain a comprehensive understanding of the size-dependent mechanical characteristics of Si NWs [11]. Another study introduces a multiscale model to bridge the existing gap between atomistic simulations and experimental observations encountered around 10 nm critical dimension [12]. Furthermore, the importance of nanomechanical model selection is highlighted, where deviations of up to 85-100 GPa in elastic properties of Si NWs are attributed to the specific choice of the model [11, 27]. In light of the existing challenges in fabrication, testing, and characterization, modeling continues to be a crucial element in precise interpretation of the findings [11, 18]. Additionally, the disparities between experimental and computational approaches concerning the scale effect present another significant challenge in this field [15, 16]. Molecular dynamics (MD) and density functional theory (DFT) play vital roles in revealing the size-dependent trends in the elastic properties of Si NWs [22, 28, 29, 27, 30]. In line with this, MD simulations are used to subject Si NWs to tensile [12, 22, 30, 31, 32], vibration [33, 34], and bending tests [27, 35, 36], providing valuable insights into their mechanical properties. Thus, utilizing small-scale modeling methods can facilitate both analytical and experimental analyses to enhance the understanding of research outcomes [12].

The convergence between high-throughput computing and advanced machine learning (ML) algorithms has introduced a novel approach for enhancing the structural design and performance of nanomaterials [37, 38, 39, 40]. This innovative approach has made a significant impact on the discovery of new materials [41, 42, 43]. While atomic-scale modeling has made remarkable progress, they still face inherent limitations due to the substantial computational expenses associated with explicit methods like MD and DFT [41, 44]. Conversely, the field of NEMS design and industrial applications necessitate a more efficient and expeditious solution to address the size effect on the elasticity of Si NWs [11]. Given the current computational challenges encountered in investigating the size effect in Si NWs, ML presents an opportunity to streamline this process and inject a new level of realism into the field of material science and technology [45, 46, 47]. Moreover, ML can function as a tool to offer enhanced understanding of material behavior at the nanoscale and to provide insights for the design purposes [48]. Additionally, ML-based techniques are not only employed to explore material properties but are also harnessed for the creation of novel interatomic potentials for Si,

offering a high degree of accuracy when compared to DFT studies [49, 50].

The current study addresses the size-dependent elastic properties of Si NWs using ML-driven atomistic simulations. The details associated with atomistic simulations are discussed in Section 2.1, while Section 2.2 addresses the specifics of ML modeling efforts. The results section offers an in-depth examination of atomistic findings given in Section 3.1 and ML-driven discoveries in Section 3.2. Ultimately, Section 3.3 provides an interpretation of the ML-based atomistic findings while exploring the potential for future expansion of the methodology introduced in this study [51]. This work contributes valuable insights into the elastic properties of Si NWs, thereby enhancing our understanding of their mechanical characteristics at the nanoscale. The developed methodology has the potential to pave the way for comparing ML-based computational results to experimental findings, serving as the benchmark and validation measure for the quality of similar efforts [11, 12, 16, 41, 47].

2. Materials and Methods

This section covers the methodology of the study in two parts: the initial one discuss the computational aspects on the modeling of Si NWs using MD simulations, while the subsequent section offers an extensive explanation of ML strategies. This includes discussions on data preparation, feature selection, and the algorithms employed within the framework of this article. An in-depth exploration of both approaches in Sections 2.1 and 2.2 are given, presenting a thorough analysis of the methods utilized.

2.1. Atomistic Simulations

This section offers a comprehensive account of modeling the tensile test of Si NWs using MD simulations. The two commonly employed boundary condition (B.C.) approaches for modeling the tensile behavior of NWs are examined: i) non-periodic and ii) periodic tensile. Sections 2.1.1 and 2.1.2 are dedicated to discussing these two approaches individually. Furthermore, both sections delve into the specifics of various computational configurations, including the preparation of atomic configurations, interatomic potentials, and other relevant computational particulars.

2.1.1. Non-periodic Tensile Simulation

In this subsection, the atomistic methodology employed for the exploration of the tensile behavior of Si NWs utilizing a non-periodic B.C. along

the NW is explained. MD simulations are conducted on Si NWs with unreconstructed surface states, utilizing the LAMMPS code [52]. Figure 1 (a) illustrates the initial atomic configuration of Si NWs, emphasizing the geometric characteristics of the NW, which possesses a square cross-sectional shape. This representation includes the width, which serves as a representation of the critical dimension (CD) in Si NWs. Figure 1 schematically describes the tensile modeling approach where the length (L) of Si NW and the fixed and movable boundaries are labeled as L_f and L_m, respectively. The lengths L_f and L_m correspond to one-eighth of the NW length (L). In this respect, the length to CD ratio (L/CD) is termed as the aspect ratio (AR). Regarding the geometrical and computational details, Table 1 provides a complete description of input parameters. In this respect, the CD spans from 2 nm to 10 nm, while the predefined ARs are assigned as 7, 8, 9, 10, 12, 14, 16, 18, and 20. Si NWs having $< 100 >$, $< 110 >$, and $< 111 >$ crystal orientations are subjected to tensile test where the interactions between Si atoms are modeled using the Tersoff-T3 (TT3) [53] and Stillinger-Weber (SW) [54] potentials. Comprehensive details of the potential expressions and coefficients are available in the respective references [53, 54].

Non-periodic B.C.s are imposed in all directions (x, y, and z) to account for a finite size. An energy minimization step is executed using the conjugate gradient method, followed by assigning an initial velocity distribution based on a finite temperature to all atoms. Subsequently, a relaxation process is carried out for 60 ps at a constant temperature, employing a 1 fs time step in the canonical NVT ensemble. During relaxation, the fixed and movable regions connected to the NW remain in fixed configurations. The subsequent tensile test involves fixing one end of the NW (L_f) while allowing the other end (L_m) to move. To mitigate shock wave generation due to rapid loading, a linearly increasing constant velocity is applied along the longitudinal direction (x). The velocity starts from zero at the support and gradually increases to its maximum at the movable boundary. A velocity of 1.0 Å/ps is applied at a constant temperature, corresponding to a strain rate of $\dot{\epsilon} \approx 1.0 \times 10^9$ s^{-1}. This rate aligns with the strain rate employed in previous MD-based tensile tests on NWs [22, 28, 30, 32]. The simulations are carried out at three distinct temperatures: specifically, 10 K, 300 K, and 600 K. The Virial theorem [55] is employed for stress calculations given in Eqn. 1.

$$\pi_{ij} = \frac{1}{2\Omega_0}\Big[\sum_{\alpha=1}^{N}\sum_{\beta\neq\alpha}^{N}\frac{1}{r^{\alpha\beta}}\frac{\partial V(r^{\alpha\beta})}{\partial r}(v_i^{\alpha\beta}v_j^{\alpha\beta})\Big] \tag{1}$$

Here, Ω_0 represents the atomic volume in an undeformed system, where N denotes the total number of atoms. The distances between atoms α and β are denoted as $r^{\alpha\beta}$. Furthermore, v_j^{α} signifies the position of atom α along the j direction, which can be expressed as $v_j^{\alpha\beta} = v_j^{\alpha} - v_j^{\beta}$. The term V corresponds to the interatomic potential. The virial stress can be calculated by summing contributions from all atoms (and atom pairs) within the simulation cell, and subsequently dividing the result by the cell volume, which in this context corresponds to the volume of the NW.

2.1.2. Periodic Tensile Simulation

This subsection outlines the MD approach used to investigate the tensile behavior of Si NWs with unreconstructed surfaces and periodic B.C.s applied along the NW. Similar to the Si NWs described in Section 2.1.1, atomistic simulations are carried out on Si NWs with crystal orientations listed in Table 1, utilizing the LAMMPS code [52]. In contrast to the Si NWs discussed earlier, periodic B.C.s are applied along the x-direction, while the y- and z-directions are constrained to model an infinitely long NW segment given in Figure 1 (c). The parameters such as CD, AR, interatomic potential, and temperature are repeated for Si NWs studied using this method. The MD simulations start with an energy minimization step using the conjugate gradient method, followed by the assignment of initial velocities based on a Gaussian distribution at the specified temperature. Subsequently, dynamic equilibration at the designated temperature is carried out for 60 ps, utilizing the Nose-Hoover isobaric-isothermal (NPT) ensemble with a time step of 1 fs. Following equilibration, the simulation cell undergoes longitudinal deformation at a strain rate of $\dot{\epsilon} = 1 \times 10^9 s^{-1}$, which falls within the suitable range for MD-based tensile testing [22, 32], as well as for Si NWs discussed in Section 2.1.1. This ensures consistency in the deformation of Si NWs within the scope of this study. The stress-strain curves obtained for Si NWs are utilized to determine the modulus of elasticity, employing the formulation given in Eqn. 1.

Apart from Si NWs featuring unreconstructed surfaces modeled in this study, the comprehensive framework also encompasses Si NWs with native

oxide surface states, as previously investigated by the authors [22, 28, 30]. In this regard, readers are encouraged to refer to the provided references in Table 1 for computational details on modeling Si NWs with native oxide [22, 28, 30].

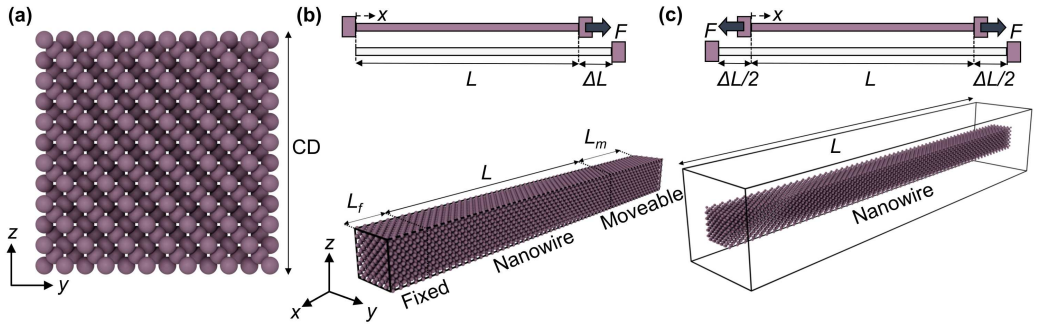

Figure 1: (a) Cross-sections of a Si NW with dimensional parameter defined as CD, representing NW width. (b) Non-periodic tensile simulation of Si NWs exhibited schematically (upper) and with atomic configuration (lower). The associated NW length (L) and B.C.s regions are referred as fixed (L_f) and movable boundaries(L_m). (c) Periodic tensile simulation of Si NWs exhibited schematically (upper) and with atomic configuration (lower). The associated NW length (L) and simulation box are shown. The force denoted by F schematically illustrates the direction of the tensile simulations.

2.2. Machine Learning

This section encompasses the intricacies related to data extraction from modeling Si NWs with unreconstructed surface states, as elaborated in Section 2.1, and draws upon information available in the literature for Si NWs with a native oxide surface state [22, 28, 30]. Further explanations regarding the data will be presented in Section 2.2.1, while details pertaining to feature selection and the implementation of ML models will be discussed in Section 2.2.2 and Section 2.2.3, respectively.

2.2.1. Data Preparation

Effective data preparation is crucial for developing a robust ML algorithm, where the relevance of data is as important as the quantity for successful predictions. To construct the dataset necessary for training the ML algorithms, two primary sources of input are employed. The modeling efforts outlined in Section 2.1 generate tensile responses for Si NWs under different parameter sets, with a specific focus on Si NWs featuring the unreconstructed surface

state. In light of three crystallographic orientations of Si, two distinct interatomic potentials, three designated testing temperatures, and nine differing Si NW CDs, coupled with nine distinct ARs modeled via non-periodic and periodic B.C.s, a comprehensive collection of 2916 Si NWs is established within this study. Additionally, data from previous research conducted by the authors on Si NWs with a native oxide surface state, as documented in relevant literature [22, 28, 30], are assimilated into the overall dataset.

The Si NWs featuring a native oxide surface state exhibit variations in critical dimension, native oxide layer thickness, applied B.C.s (non-periodic and periodic), temperature, and interatomic potentials (Tersoff-Munetoh (TM) [56] and modified Stillinger-Weber (m-SW) [57]). Notably, two key distinctions arise upon integrating data from Si NWs with these distinct surface conditions. Firstly, the unreconstructed Si NWs maintain their original surface thickness without any native oxide layer, whereas the Si NWs with native oxide exhibit values that account for differing oxide layer thicknesses. Secondly, recognizing the structural deviations resulting from oxygen atom presence in Si NWs with native oxide surfaces, a consolidation is performed concerning the categorization of Tersoff and SW potentials. Consequently, TT3 and TM, as well as SW and m-SW, are grouped within the same potential family, and comparable values are attributed during dataset preparation. In this context, the Tersoff (TT3 [53] and TM [56]) and Stillinger-Weber (SW [54] and m-SW [57]) represent two distinct families of interatomic potentials within the framework of this article. With the inclusion of the dataset pertaining to Si NWs with native oxide surface states, a total of 305 additional data points are appended to this study's collection. This extension elevates the overall number of data points to 3221, each representing the modulus of elasticity of a unique Si NW.

Certainly, acquisition a substantial number of data points stands as a primary challenge in materials informatics, primarily due to the computational costs associated with acquiring materials and their corresponding target variables. Consequently, datasets frequently comprise a limited quantity of data points. Notably, to the best of our knowledge, the number of data points available for different Si NWs, specifically those investigating elasticity using MD (excluding those presented by the authors [22, 28, 30]), is currently less than 300. This circumstance might contribute significantly to the well-recognized discrepancies between elastic properties of Si NWs obtained via computational and experimental approaches [15, 16]. In this context, every data point within the dataset encompasses seven distinct features, as delin-

eated in Table 1, along with a single target variable representing the modulus of elasticity of the Si NW. The tabulated features encompass crystallographic orientation (ORNT), CD, AR, interatomic potential (POT), temperature (T), BC (non-periodic and periodic), and surface state (SS). Each unique combination detailed in Table 1 for the unreconstructed surface condition is simulated, and the dataset is further enriched through the incorporation of Si NWs with native oxide surface states from pertinent literature [22, 28, 30]. In the context of ML applications, the intrinsic nature of predictors within the dataset might necessitate preprocessing to enhance the overall performance of the ML process. Specifically, variables within a dataset can exhibit non-normal distributions or disparate scales, all of which can adversely impact the efficacy of ML algorithms. Therefore, prior to training, an in-depth analysis of the dataset will be undertaken to comprehend the data distribution and subsequently implement suitable data transformation techniques. Through data transformation, the variables are normalized and scaled to ensure equitable treatment by ML algorithms. In this study, a z-score normalization (standardization) approach is employed to achieve standard scaling and normalization of features, ensuring a mean of zero and a standard deviation of one. In this regard, min-max scaling is applied to normalize the numerical features, ensuring that all values were scaled between 0 and 1, which could enhance the performance and convergence of the ML models. For the categorical variables (POT and BC), label encoding is used, assigning each category a unique integer value, allowing the models to efficiently process the data without being influenced by any ordinal bias. The next section will cover the details associated with descriptors and feature selection for ML algorithms.

2.2.2. Feature Selection

A meticulous feature selection process is carried out prior to constructing the dataset. Previous studies by the authors on Si NWs with native oxide surfaces [22, 30] highlighted the most important parameters to prioritize in modeling efforts for reliable ML analysis. Building on the previous findings, priority was given to parameters that significantly influence the elastic properties (more than 10% change in modulus of elasticity). The seven parameters outlined in the earlier section, along with their detailed descriptions in Table 1, have been identified as essential for this task. In this regard, highly correlated features are excluded from this scheme, as they would redundantly convey a shared realm of information. For instance, this

applies to combinations such as strain rate and time step within the context of tensile modeling of Si NWs. Despite the selection of seven features for this study, the assessment of correlation between these features is crucial, considering both linear and non-linear perspectives. To address the potential linear correlation, the Pearson's correlation coefficient (PCC) is calculated [58]. To address broader correlation issues, the random forest (RF) method, renowned for its efficacy in classification and regression tasks, is also utilized for feature correlation study [59]. In contrast to alternative feature selection methods, the RF method assigns importance scores to variables by ranking them based on their performance during model optimization. This approach allows for a comprehensive evaluation of feature correlations, facilitating enhanced interpretation of findings. Before implementing ML algorithms for data generation, the initial focus revolves around refining the dimensionality of the dataset by emphasizing the most pertinent features. From a modeling perspective, this entails considering factors like time step, cross-section shape, alternative testing methods such as bending or compression, and different types of interatomic potentials like the Modified Embedded Atom Method (MEAM) potential [31]. However, while this approach could enhance the dataset, it carries the risk of introducing an excessive number of input features, potentially leading to overfitting especially when dealing with a limited number of instances due to the problem's potential high degree of freedom or non-linearity. The following section will address the specifics pertaining to ML algorithms.

2.2.3. Machine Learning Algorithms

Building upon the insights gained from the initial data inspection via MATLAB [60] (details are given in Supporting Information), various ML algorithms namely, Random Forest Regressor (RF), K-Nearest Neighbors Regressor (KNN), Linear Regression (LR), Decision Tree Regressor (DT), Multi-Layer Perceptron Regressor (MLP), and Support Vector Regressor (SVR) are assessed in their ability to forecast the target variable. Prior to model training, the original dataset is divided into training data, facilitating model optimization, and a test dataset, employed to gauge the models' predictive accuracy on unseen data. The evaluation of ML models is grounded in their predictive errors on the test dataset, measured by root mean squared error (RMSE), mean absolute error (MAE), and coefficient of efficiency (R^2) as defined by Equations 2, 3 and 4, respectively. In this regard, y_i and $\tilde{y}_i$ are true and predicted values, respectively. Here $\bar{y}$ is the average of the pre-

Table 1: Summary of input and output parameters used for modeling the tensile behavior of Si NWs.

Definition	Descriptor	Values	Output (E) Range (GPa)
Crystal Orientation	ORNT	$< 100 >$: [100]-x [010]-y [001]-z	54.4 - 140.6
		$< 110 >$: [110]-x [001]-y [$\bar{1}$10]-z	65.9 - 211.7
		$< 111 >$: [111]-x [1$\bar{1}$0]-y [$\bar{1}\bar{1}$2]-z	67.4 - 226.6
Critical Dimension	CD	2, 3, 4, 5, 6, 7, 8, 9, 10 nm	54.4 - 226.6
Length to Width Ratio	AR	7, 8, 9, 10, 12, 14, 16, 18, 20	54.4 - 226.6
Interatomic Potentials	POT	Tersoff (TT3 [53] and TM [56]) & Stillinger-Weber (SW [54] and m-SW [57])	54.4-226.6 (Tersoff) & 67.8 - 195.3 (SW)
Temperature	T	10, 300, 600 K	54.4 - 217.9 (10K) & 54.8 - 220.3 (300K) & 61.5 - 109.0 (600K)
Boundary Conditions	BC	Non-periodic (NP) and Periodic (P)	54.8 - 226.6 (NP) & 54.4 - 183.9 (P)
Surface State	SS	Unreconstructed and Native Oxide (Refs. [22, 28, 30])	54.4 - 226.6

dicted values and n is the total number of the samples. All computations are executed using the scikit-learn library within the Python programming language [61]. Upon identifying the most effective models, additional optimization techniques, including hyperparameter tuning, are experimented with to determine optimal configurations. These optimizations are iterated to enhance the training process and mitigate the risk of overfitting given the current training dataset.

$$RMSE = \sqrt{\frac{1}{n}\sum_{i=1}^{n}(y_i - \tilde{y_i})^2} \tag{2}$$

$$MAE = \frac{1}{n}\sum_{i=1}^{n}|y_i - \tilde{y_i}| \tag{3}$$

$$R^2 = 1 - \frac{\sum_{i=1}^{n}(y_i - \tilde{y_i})^2}{\sum_{i=1}^{n}(y_i - \bar{y})^2} \tag{4}$$

3. Results

The section begins by presenting the particulars concerning the MD modeling, including the outcomes of atomistic assessments for predicting the modulus of elasticity in Si NWs as discussed in Section 2.1. It explores the intricacies of the dataset, furnishing additional insights into the data arrangement intended for the following phase of the results section (Section 3.1). Subsequently, the results of the ML approach, carried out using Python (discussed in Section 2.2), are elaborated (Section 3.2). Finally, the interpretation of findings on the elastic properties of Si NWs will be carried out in Section 3.3.

3.1. Atomistic Results

Utilizing atomistic simulations, particularly MD, presents a viable approach for investigating the elastic properties of Si NWs. Despite an extensive literature examining factors like crystallographic orientation, critical dimension, cross-section shape, AR, testing method, strain rate, temperature, interatomic potential, surface condition, defects or flaws, and B.C.s,

a consensus regarding the size effect in elasticity of Si NWs is still missing. This stems not only from disparities between computational and experimental efforts but also from significant deviations observed in atomistic findings due to variations in aforementioned parameter selection. Moreover, given the extensive applications of Si NWs in future electronics and NEMS, there is an imperative need for a rapid and precise exploration of elasticity concerning size effects. In this context, the integration of ML algorithms with computational approaches has the potential to streamline this process. This section presents the outcomes of MD simulations conducted within the scope of this paper, as well as previous data points from studies published by the authors. Within this framework, the modulus of elasticity of Si NWs is derived from stress-strain curves as the output parameter. This comprehensive analysis includes data from 2916 Si NWs modeled in this study, along with an additional 305 data points extracted from prior research by the authors [22, 28, 30]. This accumulation results in a dataset comprising 3221 data points, each representing the modulus of elasticity for a unique Si NW.

Given the computational demands associated with modeling Si NWs with a native oxide layer due to the increased number of atoms involved, the primary focus of modeling efforts is directed toward unreconstructed Si NWs. Specifically, all possible combinations of Si NWs with unreconstructed surface states, accounting for the nine different CDs, nine various ARs, three distinct temperatures, two types of B.C.s, and two types of interatomic potentials are simulated. This extensive dataset serves as a valuable resource for ongoing and prospective studies, considering its unique size and composition. The dataset presented within this section will undergo examination and analysis through the utilization of ML models in two distinct stages given in Section 3.2.

3.2. Machine Learning Results

Following the initial data set examination within the context of ML algorithms (via MATLAB provided in Supporting Information), the Python scikit-learn library is employed to conduct a more detailed investigation of elasticity in Si NWs. This analysis involves the assessment of various ML algorithms, namely RF, KNN, LR, DT, MLP, and SVR while different training data percentages, ranging from 30% to 90% with 10% intervals, are used in this evaluation. Given the size of dataset in this study, it is important to split the data thoughtfully, aiming for a balanced distribution in both the

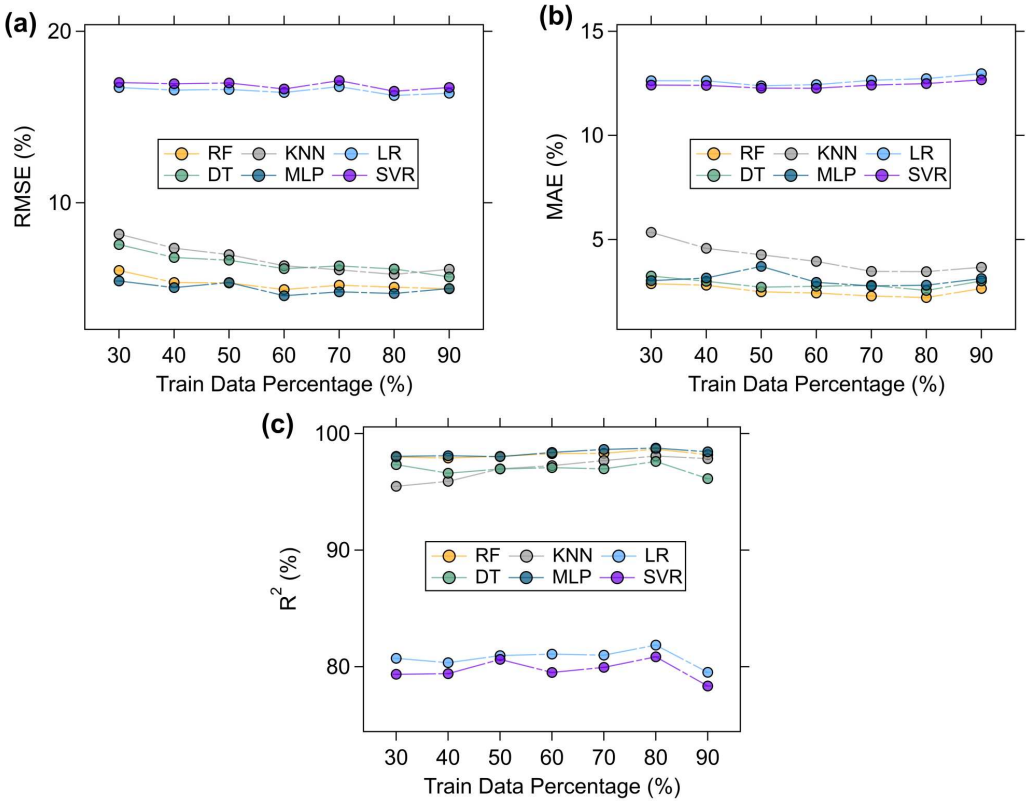

Figure 2: The evolution of (a) RMSE, (b) MAE, and (c) R^2 on test dataset with changing training dataset proportions for the RF, KNN, LR, DT, MLP, and SVR algorithms.

training and test datasets to avoid overfitting. To ensure robustness, the random assignment of the data set for this analysis is repeated across 100 trials. The ML models are evaluated based on their prediction errors on the test dataset. Subsequently, calculations of RMSE, MAE, and R^2 are performed, with their respective standard deviations presented in Figures 2 (a), (b), and (c), respectively. The obtained errors for RMSE, MAE, and R^2, based on 100 repetitions of the analysis at different training data percentages, show a negligible standard deviation, indicating the reliability of the reported errors.

When considering RMSE as the most critical performance evaluation parameter in the context of ML algorithms, a clear distinction emerges in the errors obtained. Specifically, four models – RF, KNN, MLP, and DT – report RMSE values below 10%, while LR and SVR, which both employ linear kernels in this study, exhibit higher RMSE values. This emphasizes the

non-linearity of the problem when examining the elasticity of Si NWs. Furthermore, MAE, a common measure of forecast error in time series analysis, confirms the findings from the RMSE analysis, showing a greater dependence on the training data percentage for smaller data subsets. In this context, the calculation of R^2 provides an additional quantitative assessment of the observation of non-linearity. Linear models exhibit a degree of correlation of approximately 80% within the context of prediction and target values, while the remaining four models (RF, KNN, MLP, and DT) demonstrate more than 95% coefficient of efficiency, underscoring their suitability for this task. The evaluation of uncertainty, as presented through RMSE, MAE, and R^2 in Figures 2 (a), (b), and (c), demonstrates that the majority of models exhibit the lowest error when 70% of the data is used for training, indicating this as the optimal percentage for follow-up analysis. Accordingly, the discussion on the specific models and hyperparameter analysis will focus on this data combination. Preliminary analysis using MATLAB models (given in Supporting Information) allowed for an initial evaluation of different ML models. For instance, the RF-Bagged model demonstrated lower RMSE and MAE compared to the RF-Boosted model. Therefore, the Python-based analysis is guided by these initial findings from MATLAB.

Following the discussion on error analysis, a subsequent examination and discussion of algorithms are carried out using a 30% test data percentage, which corresponds to optimal error rates observed for the majority of the trained models. Furthermore, the performance of the KNN algorithm hinges on the value of the hyperparameter K, which defines the number of closest neighbors considered from the training dataset when making predictions for a new data point. This provides an opportunity for further improvement of the KNN model where the K hyperparameter can be fine-tuned. Lower values of K such as those close to 1, result in predictions that closely resemble the patterns in the training data, reducing flexibility but potentially increasing generalization capabilities. In contrast, higher values of K introduce more diversity in the neighbor selection process. In this context, Figure 3 (a) displays the RMSE across a range of K hyperparameter values, spanning from 1 to 20. The optimal value of K is identified as 4, corresponding to the minimum error achieved. Furthermore, the paper explores the application of the bagging ensemble technique to enhance the stability and accuracy of the KNN model. The reduction in RMSE percentages for various training data percentages is illustrated in Figure 3 (b), demonstrating the benefits of this technique in improving model performance.

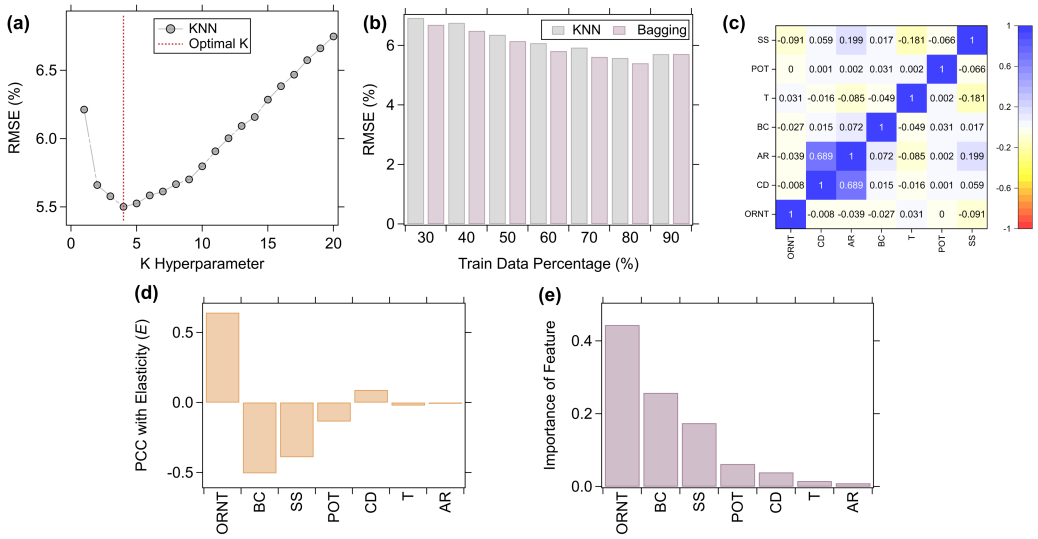

Figure 3: (a) The change in RMSE with increasing K hyperparameter for KNN algorithm. (b) Estimation of RMSE with bagging method while compared with KNN algorithm. (c) The heatmap of PCCs for associated features disucssed in Table 1, The higher color intensities exhibit the enhanced correlation between the two features while the blue and red colors indicate positive and negative correlation, respectively. (d) The PCC for for descriptors associated with the outline parameter as modulus of elasticity (E). (e) The relative feature importance for input variables based on their performance obtained via the RF method.

Furthermore, Figure 3 (c) displays a heatmap illustrating the PCCs among the input variables. Notably, the parameters representing dimensionality, specifically CD and AR, exhibit the highest correlation, reaching approximately 0.7. This correlation represents the strongest linear relationship among all the features. However, it's essential to acknowledge the limitations of the PCC method, as it disregards model performance variations and overlooks non-linear relationships among variables. Consequently, reliance on importance calculations based on the RF method is considered to be more reliable. In this context, it is important to note that the BC (second most importance feature given in Figure 3 (d)) pertains to the computational methodology employed and is not completely correlated to the physical interpretation of properties in Si NWs.

Upon initial examination of the performance of ML models on the dataset, the significance of features becomes more pronounced. The RF method, which utilizes a forest of numerous trees, is particularly adept at this task.

One notable advantage of RF is its ability to provide feature importance, making it an appealing tool for potential follow-up analyses, such as partial dependence analysis between features. Additionally, the output parameter, modulus of elasticity, has been examined using Pearson correlation analysis, with the results displayed in Figure 3 (d). The feature importance results obtained from the RF algorithm in this study are depicted in Figure 3 (e). Among these features, the crystallographic orientation, ORNT, the boundary condition definition during testing, BC, and surface state, SS, emerge as the most crucial parameters, showcasing the highest importance within the context of this problem. Conversely, the numerous simulations conducted on geometric properties, including CD and AR, exhibit lower importance when compared to the previously mentioned features. This observation is consistent with earlier research, which emphasizes the significant impact of surface effects and crystal orientation on the mechanical properties of Si NWs [11, 18, 22, 28, 27, 30]. The BC and SS emerged as critical factors in this study due to their significant influence on the elastic properties of Si NWs. BC distinguishes between periodic and non-periodic boundary conditions, each contributing differently to stress and elastic behavior. Similarly, the ss parameter, which quantifies oxide thickness, provides key insights into how surface state affects mechanical properties of Si NWs.

As depicted in Figure 4, the performance of six algorithms in predicting the modulus of elasticity of Si NWs, as a function of the actual modulus of elasticity obtained via MD simulations, is showcased. Given the performance disparities among various ML models, particularly when excluding the linear models (LR and SVR) from consideration within the scope of this study, it becomes essential to conduct a more detailed examination of these models. To ensure robustness and prevent overfitting, a ten-fold cross-validation approach is employed. Among these algorithms, the RF and DT models emerge as the top performers, followed by KNN and MLP. In contrast, LR and SVR with linear kernels exhibit the least favorable performance. Further examination of the best-performing models involves hyperparameter tuning, particularly for the RF model. This fine-tuning is implemented to control the maximum depth of individual trees, mitigating the risk of overfitting, while also governing the minimum sample leaf and minimum sample split parameters. Through this process, the following hyperparameter values are determined for the RF model: a maximum depth of 10, a minimum sample leaf of 1, and a minimum sample split of 5. This optimization results in a notable improvement, with a 0.3% reduction in RMSE, a 0.2% reduction

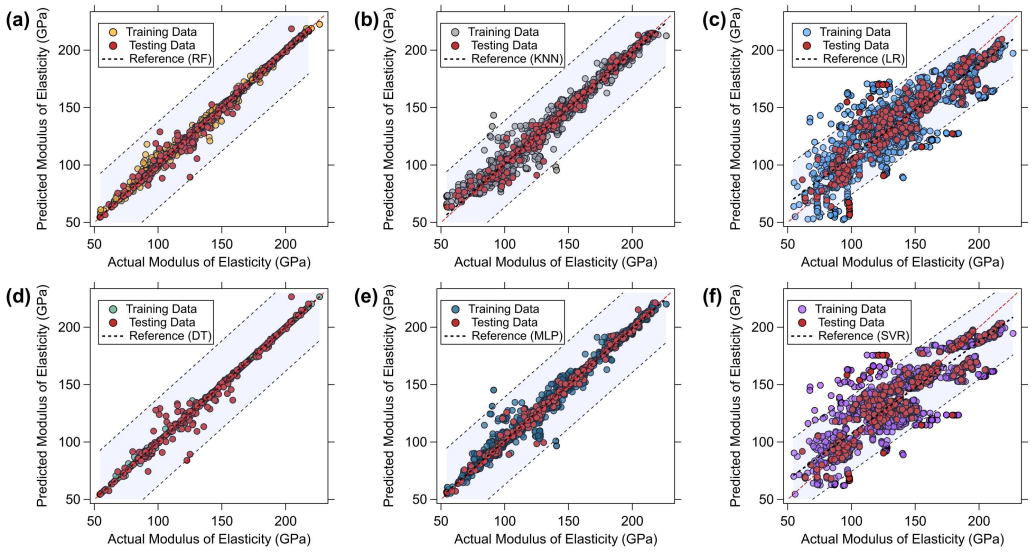

Figure 4: Performance of (a) RF, (b) KNN, (c) LR, (d) DT, (e) MLP, and (f) SVR algorithms in predicting modulus of elasticity as a function of actual modulus of elasticity available in the testing set. The line of references, along with their corresponding standard deviations, is also provided for each model. The dashed red line indicates the linear relationship between actual and predicted values, providing a clear reference for examining their correlation.

in MAE, and a 0.2% increase in R^2. Similarly, a detailed analysis of hyperparameters for the DT model is carried out, leading to the selection of the following values: a maximum depth of 10, a minimum sample leaf of 3, and a minimum sample split of 5. This hyperparameter tuning results in a 0.6% reduction in RMSE, a 0.1% reduction in MAE, and a significant 0.8% increase in R^2. These findings underscore the importance of hyperparameter tuning in optimizing the performance of ML models, particularly for decision tree-based algorithms like RF and DT. Given this, a more thorough analysis of the two most important features – crystallographic orientation (ORNT) and surface state (SS) – is necessary. Section 3.3 of the paper will present the results of such analysis based on the feature importance. In this regard, the hyperparameters used in the ML models are listed in the Supporting Information.

3.3. Interpretation of Results

This section is dedicated to interpreting the outcomes of the ML-based analysis of the MD simulations conducted on Si NWs, with a particular focus

on the areas where ML can address existing gaps in the literature. As previously discussed, the size-dependent behavior of the modulus of elasticity remains an ongoing research challenge, lacking a definitive answer regarding the size effect. Considering various effective parameters, crystal orientation, dimensionality, and surface state prove to be notably challenging. One crucial aspect of the analysis presented here is the interpretation of partial dependence between the surface state and crystal orientation of Si NWs. These two features stand out as the most impactful, disregarding the influence of BC, which mainly mirrors computational methodology and does not directly represent the modulus of elasticity in Si NWs. Furthermore, once ML algorithms achieve a reliable level of performance, they can serve as efficient tools for predicting the surface state and Si NW orientation, facilitating the rapid estimation of the modulus of elasticity.

Focusing on four models, specifically the KNN, MLP, DT, and RF, which have demonstrated superior performance in this study, this section explores the partial dependence of surface state on three crystal orientations of Si NWs. These relationships are visualized in Figures 5 (a), (b), (c), and (d), respectively. It is noteworthy that each model exhibits a distinct trend in prediction, influenced by the level of non-linearity, spanning across the three crystal orientations and the provided range of surface states. For the analysis presented in Figures 5 and 6, the temperature was consistently maintained at 300K, reflecting standard experimental conditions. This ensures that variations in the observed results are attributed to changes in surface thickness and crystallographic orientations, while the remaining parameters vary within the associated ranges presented in this work. Rather than identifying a single, most successful model, the results depicted in Figure 5 offer a valuable and prompt method for estimating the modulus of elasticity for Si NWs. In light of the discrepancies between experimental findings and computational results when addressing the size effect in the elastic properties of Si NWs, Figure 5 serves as an initial step towards a more informed interpretation of the elastic response in Si NWs. It provides a promising foundation for an intelligent roadmap towards understanding the behavior of Si NWs in terms of their modulus of elasticity. To the best of our knowledge, such an approach has not been reported previously. While the current study employs empirical interatomic potentials to maintain consistency with existing literature, the increasing significance of ML-based potentials is clear. Future research should incorporate such advanced interatomic models to further enhance the analysis of Si NWs, particularly with respect to their elastic properties, enabling a

more comprehensive comparison concerning computational and experimental findings.

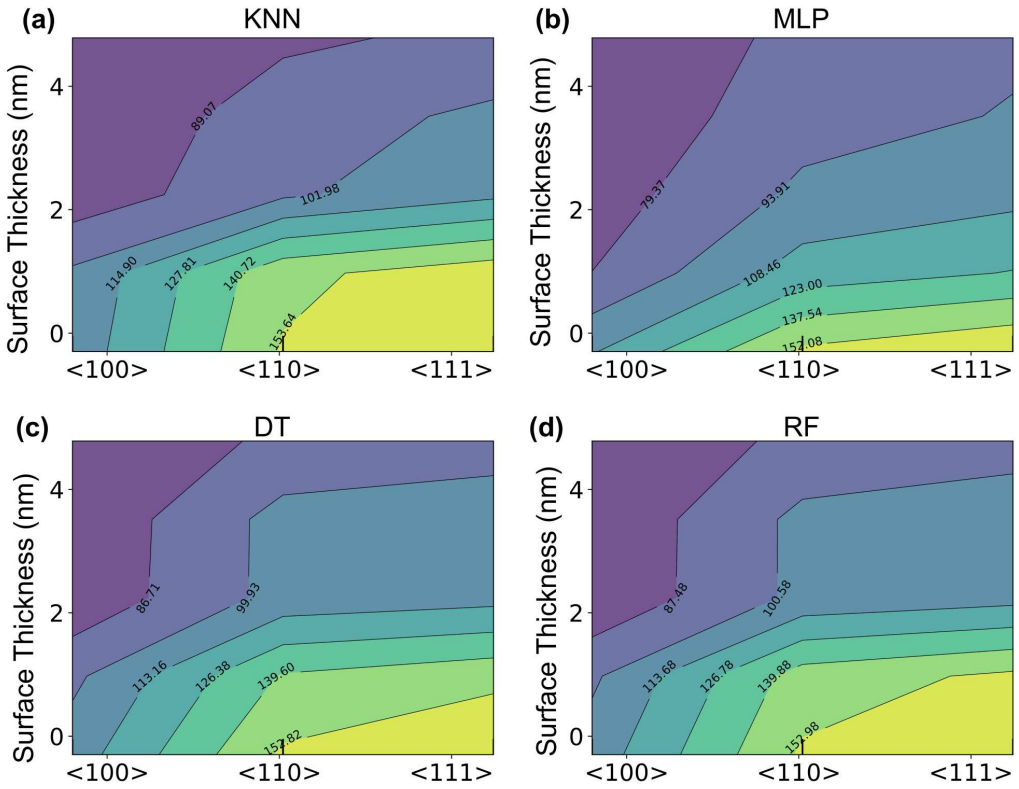

Figure 5: Partial dependence of elasticity between surface thickness and crystallographic orientation of Si NWs studied using (a) KNN, (b) MLP, (c) DT, and (d) RF models.

Given the significance of crystal orientation in Si NWs, as indicated in prior literature and in the context of this study, the common approach for characterizing the orientation of crystalline materials in a spatially resolved manner is through techniques like electron backscatter diffraction (EBSD) [62, 63, 64]. This study focuses on the utilization of inverse pole figure (IPF) coloring to assess the influence of crystal orientation on the modulus of elasticity of Si NWs. IPF offers a set of visual representations that enable the transformation of arbitrarily scattered pole figure data, a task that involves considerable mathematical and computational challenges. To address the relationship between crystal orientation and the modulus of elasticity of Si NWs, a detailed analysis based on the partial dependence calculations of four

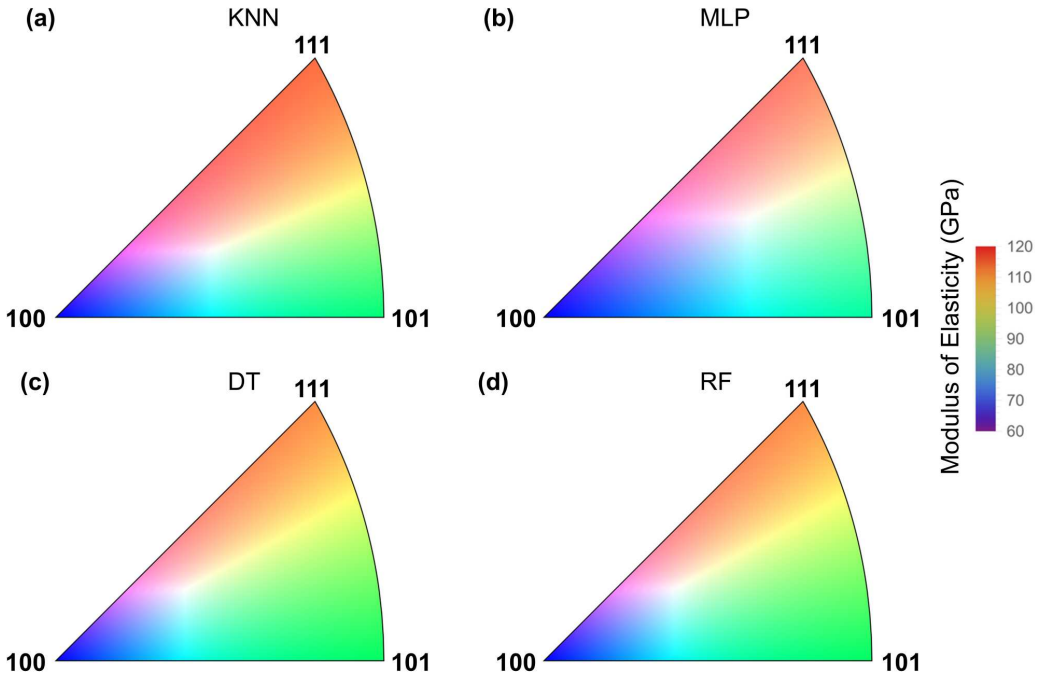

Figure 6: Crystal orientation dependence of modulus of elasticity visualized using IPF for Si NWs using (a) KNN, (b) MLP, (c) DT, and (d) RF models.

successful ML models is conducted, given in Figure 6. In this regard, the IPF visualizations for the modulus of elasticity with a constant surface thickness are presented for the KNN, MLP, DT, and RF models in Figures 6 (a), (b), (c), and (d), respectively. The shapes displayed in these figures represent stereographic projections of specific directions situated at the three corners, which correspond to the directions within the Si NWs investigated here. The various shades in the IPFs indicate varying degrees of stiffness in relation to the different orientations of Si NWs. This analysis on the orientation-dependent modulus of elasticity for Si NWs is carried out based on partial dependence analysis while maintaining a constant surface thickness, enabling the observation of variations between different ML models as different crystal orientations are examined. Considering the uncertainties associated with size dependent elastic properties of Si NWs in the literature, Figure 6 is, to the best of our knowledge, the first representation of orientation dependence within the context of elastic properties of Si NWs. In this regard, Figure 6 demonstrates the significance of scale effect while the deviations

between the ML models remain negligible. The contour lines in Figures 5 and 6, derived from the ML predictions, should be interpreted with caution, particularly in areas where lines intersect. This intersection underscores the significant uncertainty in the predicted elasticity values. For a more accurate interpretation, comparisons should concentrate on the external regions where predictions are more reliable.

4. Conclusion

This study effectively integrates atomistic modeling with ML techniques to explore and predict the mechanical properties of Si NWs, particularly their modulus of elasticity. The research utilized MD simulations to generate a robust dataset of 2916 data points (overall dataset of 3221), revealing the complex, non-linear mechanical behavior of Si NWs. By training ML models on this dataset, we achieved efficient predictions of elasticity, which facilitated the generation of detailed graphs, such as those in Figures 5 and 6. These figures illustrate the relationships between key surface state effects and orientation of Si NWs.

Key findings include:

• Optimal Data Division: A 30% test set size was identified as optimal for balancing model performance and prediction accuracy, reflecting the lowest error rates observed.

• Feature Importance: RF model highlighted surface state and crystal orientation as the most influential features in predicting elasticity. These findings underscore the significance of these features in determining the mechanical response of Si NWs.

• Model Performance: Among the models evaluated, the RF, KNN, MLP and DT models demonstrated superior performance due to their ability to capture non-linear relationships, compared to linear models like LR and SVR.

This study demonstrates the potential of combining MD simulations with ML to accelerate the understanding of Si NWs' mechanical properties, providing valuable insights for future research in nanoelectromechanical systems and nanoelectronics. While the ML models offer enhanced prediction capabilities, the associated uncertainties must be considered for data analysis.

Data Availability Statement

The data that support the findings of this study are available from the corresponding author upon reasonable request.

Conflict of Interest

The authors have no conflicts to disclose.

Acknowledgments

S.Z.P. and B.E.A. gratefully acknowledge financial support by Tubitak under grant no 120E347.

References

[1] A. Bachtold, J. Moser, M. Dykman, Mesoscopic physics of nanomechanical systems, Reviews of Modern Physics 94 (4) (2022) 045005.

[2] S. Gao, S. Hong, S. Park, H. Y. Jung, W. Liang, Y. Lee, C. W. Ahn, J. Y. Byun, J. Seo, M. G. Hahm, et al., Catalyst-free synthesis of sub-5 nm silicon nanowire arrays with massive lattice contraction and wide bandgap, Nature communications 13 (1) (2022) 3467.

[3] L. N. Quan, J. Kang, C.-Z. Ning, P. Yang, Nanowires for photonics, Chemical reviews 119 (15) (2019) 9153–9169.

[4] G. Bronstrup, N. Jahr, C. Leiterer, A. Csáki, W. Fritzsche, S. Christiansen, Optical properties of individual silicon nanowires for photonic devices, ACS nano 4 (12) (2010) 7113–7122.

[5] H. Zhang, Y. Qiu, F. Osawa, M. Itabashi, N. Ohshima, T. Kajisa, T. Sakata, T. Izumi, H. Sone, Estimation of the depletion layer thickness in silicon nanowire-based biosensors from attomolar-level biomolecular detection, ACS Applied Materials & Interfaces 15 (16) (2023) 19892–19903.

[6] S. Panda, S. Hajra, K. Mistewicz, P. In-na, M. Sahu, P. M. Rajaitha, H. J. Kim, Piezoelectric energy harvesting systems for biomedical applications, Nano Energy (2022) 107514.

[7] M. Nehra, N. Dilbaghi, G. Marrazza, A. Kaushik, R. Abolhassani, Y. K. Mishra, K. H. Kim, S. Kumar, 1d semiconductor nanowires for energy conversion, harvesting and storage applications, Nano Energy 76 (2020) 104991.

[8] F. Wang, A. Dong, W. E. Buhro, Solution–liquid–solid synthesis, properties, and applications of one-dimensional colloidal semiconductor nanorods and nanowires, Chemical reviews 116 (18) (2016) 10888–10933.

[9] S. Zare Pakzad, S. Akinci, M. Karimzadehkhouei, B. E. Alaca, Simplified top-down fabrication of sub-micron silicon nanowires, Semiconductor Science and Technology 38 (12) (2023) 125005.

[10] S. Z. Pakzad, B. Ali, S. B. Coban, M. Karimzadehkhouei, B. E. Alaca, Innovative mems stage for automated micromechanical testing, in: 2023 International Conference on Manipulation, Automation and Robotics at Small Scales (MARSS), IEEE, 2023, pp. 1–6.

[11] S. Zare Pakzad, M. Nasr Esfahani, Z. Tasdemir, N. Wollschlager, T. Li, X. Li, M. Yilmaz, Y. Leblebici, B. E. Alaca, Nanomechanical modeling of the bending response of silicon nanowires, ACS Applied Nano Materials 6 (17) (2023) 15465–15478.

[12] S. Z. Pakzad, M. N. Esfahani, B. E. Alaca, An analytical-atomistic model for elastic behavior of silicon nanowires, Journal of Physics: Materials 7 (3) (2024) 03LT04.

[13] S. Wang, Z. Shan, H. Huang, The mechanical properties of nanowires, Advanced Science 4 (4) (2017) 1600332.

[14] J. L. Mead, S. Wang, S. Zimmermann, S. Fatikow, H. Huang, Resolving the adhesive behavior of 1d materials: A review of experimental approaches, Engineering 24 (2023) 39–72.

[15] C. Yang, E. Van Der Drift, P. French, Review of scaling effects on physical properties and practicalities of cantilever sensors, Journal of Micromechanics and Microengineering 32 (10) (2022) 103002.

[16] M. Nasr Esfahani, B. E. Alaca, A review on size-dependent mechanical properties of nanowires, Advanced Engineering Materials 21 (8) (2019) 1900192.

[17] H. S. Park, W. Cai, H. D. Espinosa, H. Huang, Mechanics of crystalline nanowires, MRS bulletin 34 (3) (2009) 178–183.

[18] S. Zare Pakzad, M. Nasr Esfahani, Z. Tasdemir, N. Wollschlaeger, X. Li, T. Li, M. Yilmaz, Y. Leblebici, B. E. Alaca, A new characterization approach to study the mechanical behavior of silicon nanowires, Mrs Advances 6 (19) (2021) 500–505.

[19] A. Sofiah, M. Samykano, K. Kadirgama, R. Mohan, N. Lah, Metallic nanowires: mechanical properties–theory and experiment, Applied Materials Today 11 (2018) 320–337.

[20] K. Momeni, Y. Ji, Y. Wang, S. Paul, S. Neshani, D. E. Yilmaz, Y. K. Shin, D. Zhang, J.-W. Jiang, H. S. Park, et al., Multiscale computational understanding and growth of 2d materials: a review, npj Computational Materials 6 (1) (2020) 22.

[21] P. Müller, A. Saúl, Elastic effects on surface physics, Surface Science Reports 54 (5-8) (2004) 157–258.

[22] S. Z. Pakzad, M. N. Esfahani, B. E. Alaca, The role of native oxide on the mechanical behavior of silicon nanowires, Materials Today Communications 34 (2023) 105002.

[23] M. Nasr Esfahani, S. Zare Pakzad, T. Li, X. Li, Z. Tasdemir, N. Wollschläger, Y. Leblebici, B. E. Alaca, Effect of native oxide on stress in silicon nanowires: Implications for nanoelectromechanical systems, ACS Applied Nano Materials 5 (9) (2022) 13276–13285.

[24] P. Ye, T. Ernst, M. V. Khare, The last silicon transistor: Nanosheet devices could be the final evolutionary step for moore's law, IEEE spectrum 56 (8) (2019) 30–35.

[25] H. Ando, T. Namazu, Influence of vacuum annealing on mechanical characteristics of focused ion beam fabricated silicon nanowires, Journal of Vacuum Science & Technology B 41 (6) (2023).

[26] S. Z. Pakzad, B. Ali, M. Muzammil, U. Kerimzade, B. E. Alaca, High-throughput vibrational testing of silicon nanowires, in: 2024 International Conference on Manipulation, Automation and Robotics at Small Scales (MARSS), IEEE, 2024, pp. 1–6.

[27] S. Z. pakzad, M. N. Esfahani, B. E. Alaca, Investigation of the bending behavior in silicon nanowires: A nanomechanical modeling perspective, International Journal of Applied Mechanics 16 (07) (2024) 2450073.

[28] S. Z. Pakzad, M. N. Esfahani, B. E. Alaca, Molecular dynamics study of orientation-dependent tensile properties of si nanowires with native oxide: Surface stress and surface energy effects, in: 2021 IEEE 21st International Conference on Nanotechnology (NANO), IEEE, 2021, pp. 370–373.

[29] B. Lee, R. E. Rudd, First-principles study of the young's modulus of si $< 001 >$ nanowires, Physical review B 75 (4) (2007) 041305.

[30] S. Z. Pakzad, M. N. Esfahani, B. E. Alaca, Mechanical properties of silicon nanowires with native oxide surface state, Materials Today Communications 38 (2024) 108321.

[31] W. Xu, W. K. Kim, Molecular dynamics simulation of the uniaxial tensile test of silicon nanowires using the meam potential, Mechanics of Materials 137 (2019) 103140.

[32] K. Kang, W. Cai, Brittle and ductile fracture of semiconductor nanowires–molecular dynamics simulations, Philosophical Magazine 87 (14-15) (2007) 2169–2189.

[33] J. Kim, S. Park, J. Park, J. Lee, Molecular dynamics simulation of elastic properties of silicon nanocantilevers, Nanoscale and Microscale Thermophysical Engineering 10 (1) (2006) 55–65.

[34] S. Park, J. Kim, J. Park, J. Lee, Y. Choi, O. Kwon, Molecular dynamics study on size-dependent elastic properties of silicon nanocantilevers, Thin solid films 492 (1-2) (2005) 285–289.

[35] X. Zhuo, H. Beom, Atomistic study of the bending properties of silicon nanowires, Computational Materials Science 152 (2018) 331–336.

[36] A. Ilinov, A. Kuronen, Atomistic modeling of bending properties of oxidized silicon nanowires, Journal of Applied Physics 115 (10) (2014) 104305.

[37] A. Jain, S. P. Ong, G. Hautier, W. Chen, W. D. Richards, S. Dacek, S. Cholia, D. Gunter, D. Skinner, G. Ceder, et al., Commentary: The materials project: A materials genome approach to accelerating materials innovation, APL materials 1 (1) (2013).

[38] S. Curtarolo, G. L. Hart, M. B. Nardelli, N. Mingo, S. Sanvito, O. Levy, The high-throughput highway to computational materials design, Nature materials 12 (3) (2013) 191–201.

[39] V. L. Deringer, A. P. Bartók, N. Bernstein, D. M. Wilkins, M. Ceriotti, G. Csányi, Gaussian process regression for materials and molecules, Chemical Reviews 121 (16) (2021) 10073–10141.

[40] A. Catal, E. Bedir, R. Yilmaz, M. Swider, C. Lee, O. El-Atwani, H. Maier, H. Ozdemir, D. Canadinc, Machine learning assisted design of novel refractory high entropy alloys with enhanced mechanical properties, Computational Materials Science 231 (2024) 112612.

[41] V. L. Deringer, M. A. Caro, G. Csányi, Machine learning interatomic potentials as emerging tools for materials science, Advanced Materials 31 (46) (2019) 1902765.

[42] Y. Wang, M. L. Adam, Y. Zhao, W. Zheng, L. Gao, Z. Yin, H. Zhao, Machine learning-enhanced flexible mechanical sensing, Nano-Micro Letters 15 (1) (2023) 55.

[43] K. T. Butler, D. W. Davies, H. Cartwright, O. Isayev, A. Walsh, Machine learning for molecular and materials science, Nature 559 (7715) (2018) 547–555.

[44] V. L. Deringer, N. Bernstein, A. P. Bartók, M. J. Cliffe, R. N. Kerber, L. E. Marbella, C. P. Grey, S. R. Elliott, G. Csányi, Realistic atomistic structure of amorphous silicon from machine-learning-driven molecular dynamics, The journal of physical chemistry letters 9 (11) (2018) 2879–2885.

[45] R. Ramprasad, R. Batra, G. Pilania, A. Mannodi-Kanakkithodi, C. Kim, Machine learning in materials informatics: recent applications and prospects, npj Computational Materials 3 (1) (2017) 54.

[46] L. C. Erhard, J. Rohrer, K. Albe, V. L. Deringer, Modelling atomic and nanoscale structure in the silicon-oxygen system through active machine learning, arXiv preprint arXiv:2309.03587 (2023).

[47] H. J. Kulik, T. Hammerschmidt, J. Schmidt, S. Botti, M. A. Marques, M. Boley, M. Scheffler, M. Todorović, P. Rinke, C. Oses, et al., Roadmap on machine learning in electronic structure, Electronic Structure 4 (2) (2022) 023004.

[48] T. Han, N. Stone-Weiss, J. Huang, A. Goel, A. Kumar, Machine learning as a tool to design glasses with controlled dissolution for healthcare applications, Acta biomaterialia 107 (2020) 286–298.

[49] A. P. Bartók, J. Kermode, N. Bernstein, G. Csányi, Machine learning a general-purpose interatomic potential for silicon, Physical Review X 8 (4) (2018) 041048.

[50] D. Dickel, M. Nitol, C. Barrett, Lammps implementation of rapid artificial neural network derived interatomic potentials, Computational Materials Science 196 (2021) 110481.

[51] S. Zare Pakzad, M. Nasr Esfahani, D. Canadinc, B. E. Alaca, Machine learning insights into the elasticity of bottom-up silicon nanowires, Available at SSRN 4791813 (2024).

[52] A. P. Thompson, H. M. Aktulga, R. Berger, D. S. Bolintineanu, W. M. Brown, P. S. Crozier, P. J. in't Veld, A. Kohlmeyer, S. G. Moore, T. D. Nguyen, et al., Lammps-a flexible simulation tool for particle-based materials modeling at the atomic, meso, and continuum scales, Computer Physics Communications 271 (2022) 108171.

[53] J. Tersoff, New empirical approach for the structure and energy of covalent systems, Physical review B 37 (12) (1988) 6991.

[54] F. H. Stillinger, T. A. Weber, Computer simulation of local order in condensed phases of silicon, Physical review B 31 (8) (1985) 5262.

[55] J. Cormier, J. Rickman, T. Delph, Stress calculation in atomistic simulations of perfect and imperfect solids, Journal of Applied Physics 89 (1) (2001) 99–104.

[56] S. Munetoh, T. Motooka, K. Moriguchi, A. Shintani, Interatomic potential for si–o systems using tersoff parameterization, Computational Materials Science 39 (2) (2007) 334–339.

[57] P. Ganster, G. Tréglia, A. Saúl, Atomistic modeling of strain and diffusion at the si/sio 2 interface, Physical Review B 81 (4) (2010) 045315.

[58] P. Sedgwick, Pearson's correlation coefficient, Bmj 345 (2012).

[59] K. J. Archer, R. V. Kimes, Empirical characterization of random forest variable importance measures, Computational statistics & data analysis 52 (4) (2008) 2249–2260.

[60] T. M. Inc., Matlab version: 9.13.0 (r2022b) (2022).
URL `https://www.mathworks.com`

[61] F. Pedregosa, G. Varoquaux, A. Gramfort, V. Michel, B. Thirion, O. Grisel, M. Blondel, P. Prettenhofer, R. Weiss, V. Dubourg, et al., Scikit-learn: Machine learning in python, the Journal of machine Learning research 12 (2011) 2825–2830.

[62] R. Hielscher, H. Schaeben, A novel pole figure inversion method: specification of the mtex algorithm, Journal of Applied Crystallography 41 (6) (2008) 1024–1037.

[63] G. Purcek, O. Saray, M. Nagimov, A. Nazarov, I. Safarov, V. Danilenko, O. Valiakhmetov, R. Mulyukov, Microstructure and mechanical behavior of ufg copper processed by ecap following different processing regimes, Philosophical Magazine 92 (6) (2012) 690–704.

[64] R. Li, H. Chen, H. Zhu, M. Wang, C. Chen, T. Yuan, Effect of aging treatment on the microstructure and mechanical properties of al-3.02 mg-0.2 sc-0.1 zr alloy printed by selective laser melting, Materials & Design 168 (2019) 107668.